Broadband Dual-Polarized Planar Antennas for Radar With Printed Circuit Balun

Hoang Trong Mai
Center for Remote Sensing of Ice Sheets
University of Kansas
Lawrence, KS USA
h819m139@ku.edu

Fernando Rodriguez-Morales
Center for Remote Sensing of Ice Sheets
University of Kansas
Lawrence, KS USA
frodrigu@ku.edu

Abstract—**This paper demonstrates the design and implementation of two dual-polarized ultra-wideband antennas for radar ice sounding. The first antenna operates at UHF (600–900 MHz). The second antenna operates at VHF (140–215 MHz). Each antenna element is composed of two orthogonal octagon-shaped dipoles, two inter-locked printed circuit baluns and an impedance matching network for each polarization. We built and tested one prototype antenna for each band and showed a VSWR of less than 2:1 at both polarizations over a fractional bandwidth exceeding 40 %. Our antennas display cross-polarization isolation larger than 30 dB, an E-plane 3-dB beamwidth of 69 degrees, and a gain of at least 4 dBi with a variation of ± 1 dB across the bandwidth. We demonstrate peak power handling capabilities of 400-W and 1000-W for the UHF and VHF bands, respectively. Our design flow allows for straightforward adjustment of the antenna dimensions to meet other bandwidth constraints.**

Keywords— dual-polarization, broadband antenna, frequency reconfigurable, printed circuit balun.

I. INTRODUCTION

At the Center for Remote Sensing of Ice Sheets (CReSIS) at The University of Kansas (KU), USA, we are developing an improved dual-frequency radar to operate simultaneously at UHF (Band I: 600 – 900 MHz) and VHF (Band 2: 140 – 215 MHz). The system will be an upgraded version of the instruments presented in [1-2], providing dual-polarized measurement capabilities in support of glaciological studies in Polar Regions.

The radar's antenna system will consist of (i) six VHF elements aligned in the cross-track direction (perpendicular to the travel path) for imaging the ice-sheet internal structure and basal conditions [3]; and (ii) an array of 4 × 4 wideband UHF elements that provide sufficient vertical resolution to map internal layer displacement with very high precision.

Planar antennas with polarimetric capabilities are mostly constrained to LTE applications operating above 1.7 GHz [4-6]. Low-profile broadband designs (with or without integrated feed structures) suitable for dual-polarization measurements at VHF or UHF are limited in current literature [7-10]. To address the lack of an existing array design for our application, we developed a set of custom antenna elements, based on the novel broadband ±45° dual-polarized radiator with y-shaped feeding lines for 2G/3G/LTE presented in [4]. We chose this configuration because of its high gain and simple bipolarized configuration, which can support different frequencies by adjusting the dimensions of the antenna. Table I offers a summary of the key specifications of our two designs and a comparison with previous related work.

TABLE I. SUMMARY OF DUAL-POLARIZATION ANTENNA PARAMETERS AND COMPARISON WITH PREVIOUS WORK

Ref.	Frequency Range [GHz]	Gain [dBi]	Peak Power Handling [W]	Application
This work (Band I)	0.6–0.9	6±1	400	Ice sounding
This work (Band II)	0.14–0.215	4±1	1000	Ice sounding
[4]	1.7–2.7	8.2±0.6	20*	2G/3G/LTE wireless communications
[5]	1.7–2.7	8.5	20*	2G/3G/LTE wireless communications
[6]	2.3–3.6	8.5–11	20*	LTE/5G wireless communications
[7]	0.11–0.25	5	N/A	Space observations
[8]	0.25–0.45	4 (max)	N/A	Radar/communications
[9]	0.9–0.96	1 (max)	N/A	RFID
[10]	0.13–0.16	10.3 (max)	N/A	Sea ice sounding

*The highest transmit power specified for the standard supported by this design is 43 dBm (20 W) [11-13].

TABLE II. DIMENSIONS OF THE UHF ANTENNA ELEMENT

Parameter	L	L1	L2	L3
Value (mm)	2.4	34	30	30
Parameter	Ld	D	H_t	H
Value (mm)	158.25	4	2.1678	100

II. DUAL-POLARIZED ANTENNA ELEMENT OVERVIEW

A. UHF Antenna Element

The geometry of the proposed design for Band I is shown in Fig. 1a. This antenna consists of two loop radiator dipoles located on each side of a printed circuit board (PCB). The dipole arms are angled 45 degrees from each other on the horizontal surface to provide the dual polarization capability. The board is 62-mil thick, made of conventional FR4 substrate with a nominal dielectric constant of 4.4 and a loss tangent of 0.02. Each radiator takes the shape of an octagon with the side facing the intersection thinned and extended. We use a 1-mm thick aluminum sheet underneath the element to act as a ground plane/reflector. The cross-polarized elements are fed via two printed circuit baluns, with an optional impedance matching circuit to improve the input coupling. We summarize relevant dimensions of this design in Table II.

This arrangement produces two resonant frequencies. The lower resonance is created by the +45° loop radiator dipole.

The upper resonance only exists when the -45° parasitic dipole is stacked on top. Together, these two resonances determine the bandwidth of the antenna, which extends beyond that of a conventional single dipole while providing additional gain [14].

By increasing *L1* or *L2*, the lower resonant frequency shifts down, which is expected based on the length of the dipole increasing. However, the upper resonant frequency can only be changed by adjusting *L1* (the length of coupling lines between +45° and -45° dipoles) and *D* (the gap between them), essentially changing the parasitic capacitance between two dipoles [4]. Therefore, if *L1* increases or *D* decreases, the capacitance goes up, making the overall antenna's impedance more capacitive (instead of ideally resistive). Thus, the bandwidth is decreased, *i.e.*, the upper resonant frequency shifts down.

We placed the antenna element at a distance *H* above the reflector for unidirectional radiation. Conventional antenna theory dictates that *H* should ideally be a quarter-wavelength at the center frequency. In practice, *H* was tuned between 100 mm (quarter wavelength at 750 MHz) and 130 mm (quarter wavelength at 600 MHz) to achieve the best radiation performance over the entire bandwidth of interest.

The original design does not provide good enough port-to-port isolation (S_{21}) reaching a value as high as -25 dB [4]. It is crucial to minimize this mutual coupling, as it can affect the angle of arrival estimation for bed topography mapping [3]. To this end, we implemented notches along the *L1* sides of the antenna. The notches disrupt the current path along the dipole ends, thereby decreasing mutual inductance and thus coupling [12].
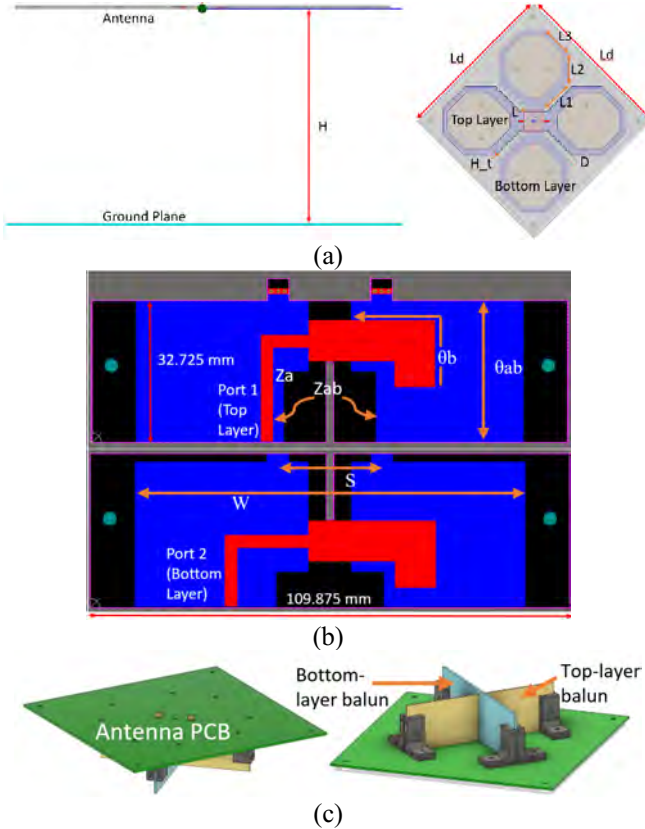

(a)

(b)

(c)

Fig. 1. Configuration of the dual-polarization UHF (Band I) antenna element with its printed baluns. (a) Layout of the antenna element and ground plane geometry. (b) Geometry of the printed balun for each dipole. (c) 3D model of the fully assembled bipolarized antenna element with balun.

Although the Y-shaped feeding lines used in the original design extend the bandwidth [4], their complex design runs against our intention of simplifying both the tuning and manufacturing processes. By using the printed circuit design balun for antenna feeding [16], it is only necessary to know the average antenna resistance *R* across the bandwidth. We determined *R* based on electromagnetic (EM) simulations, which will be discussed in Section III.

The electrical length $\theta = \theta_b = \theta_{ab}$ shown in Fig. 1b can be found using:

$$\sin^2(\theta) = \frac{Z_a}{R} \qquad (1)$$

where Z_a is the impedance of the feeding line (50 Ω). Moreover, Z_{ab} should be chosen to be as large as possible. Given the size of the board, the maximum value for Z_{ab} in this case is 185 Ω, as it depends on the ratio between the width of the ground planes on the bottom layer (*W*) and the gap between them (*S*). As for Z_b, it can be found as:

$$Z_b = \frac{R^2}{Z_{ab}} \qquad (2)$$

From here, we determined the length and width of each trace using the transmission line calculator in Keysight's Advanced Design System (ADS). The resulting baluns are shown in Fig. 1b. We mount them underneath the antenna and interlock them through a slit in middle, as shown in Fig. 1c.

B. VHF Antenna Element

Using the design principle explained in Section II.A, the Band II antenna is configured as shown in Fig. 2a, with its dimensions summarized in Table III. In order to make prototyping and testing easier given its large size, two key features of the antenna are removed here, including the non-conductive holes in each loop and the notches along L1. The first removal will produce a narrower impedance bandwidth [4]; however, the change is tolerable given the bandwidth requirements for Band II. The second removal increases the mutual inductance [15] to a point manageable by a low-order lumped element impedance matching network. The sized-up version of the baluns used with this configuration is presented in Fig. 2b. The baluns are mounted as shown in Fig. 2c.

III. SIMULATION RESULTS AND DISCUSSIONS

A. UHF Antenna Element

We completed full-wave EM simulations using Ansys' High Frequency Simulator (HFSS). Numerous tuning iterations of *L*, *L1*, *L2* and *L3* yielded a final dipole length of 174.167 mm, ~87 % of the half-wavelength (200 mm) at the center frequency. This value was used to achieve the desired performance in the initial simulation setup with the antenna element only (no balun included). However, the measurement results in Fig. 3 showed some deviation from the ideal case, with the return loss of the antenna alone being well above -10 dB across the entire bandwidth.

After determining the average simulated impedance of the system (70.58 Ω), we derived the balun dimensions by using (1) and (2). Next, we implemented the balun circuit layout using Altium Designer and then simulated it using the Momentum component of Keysight ADS. The electrical length of the 50-Ohm lines on the top-layer and bottom-layer baluns had to be adjusted to accommodate a vertical slit for

interlocking, allowing the two boards to slide orthogonally into each other. Fig. 4 demonstrates the balun performance resulting from this alteration. The top-layer balun exhibits better return loss but slightly worse insertion loss roll-off as the frequency increases.

The two orthogonal baluns present a simulated $|S_{11}|$ below -10 dB and $|S_{21}|$ between 3.5–4.5 dB over the desired bandwidth. Considering that the balun acts as a power splitter with 180° phase difference between each dipole arm, it offers an insertion loss in the 0.5−1.5 dB range. The simulated balun phase imbalance is between 2.09 and 3.52 degrees.

The measured response of the Band I antennas with baluns is shown in Fig. 5. Varying the ground plane height H indicates that the best return loss performance is achieved at H = 13 cm (approximately quarter wavelength at the lowest frequency), where the actual 10-dB bandwidth is between 606 MHz and 886 MHz. The port-to-port isolation verifies that the implemented notches work properly, making $|S_{21}|$ lower than -30 dB for most of the bandwidth − a 7-dB improvement over the original design operating at higher frequencies [4].
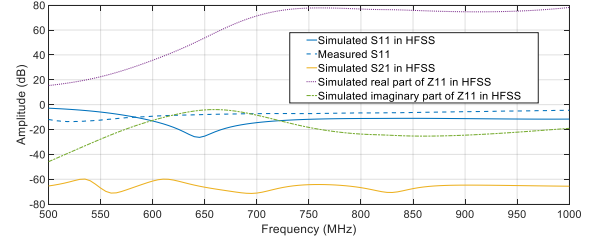

Fig. 3. Simulated and measured S-parameters of the UHF antenna element without balun.
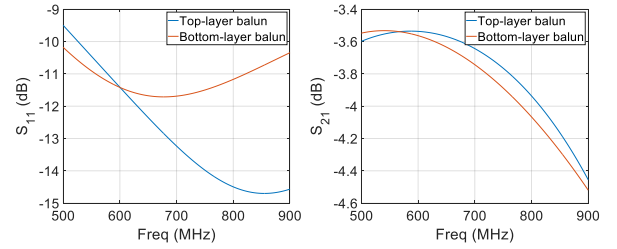

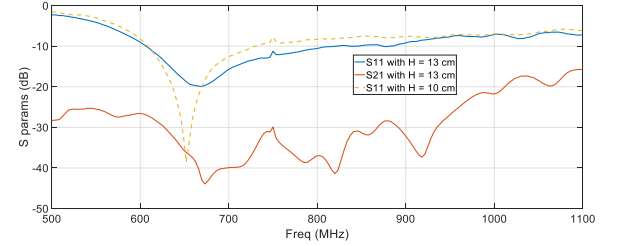Fig. 4. Simulated S-parameters of the balun design simulated in ADS.

Fig. 5. Measured S-parameters of the UHF antenna with baluns attached.
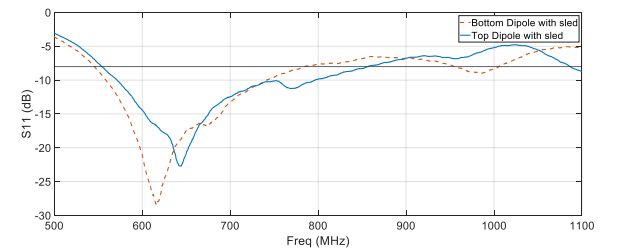

Fig. 6. The measured return loss of the UHF antenna element inside the sled enclosure (without impedance matching network).
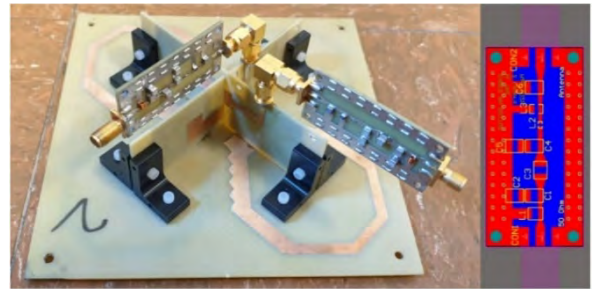

Fig. 2. Configuration of the VHF (Band II) antenna with its printed baluns. (a) Layout of the antenna element and ground plane configuration. (b) Geometry of the printed balun for each dipole. (c) 3D model of the fully assembled bipolarized antenna element with balun.

TABLE III. DIMENSIONS OF THE VHF ANTENNA

Parameters	L	L1	L2	L3
Value (mm)	10	180	125	80
Parameters	Ld	D	H	Lg
Value (mm)	700	20	550	730.25

Fig. 7. Final prototype of the UHF antenna element with attached baluns and matching networks (matching network layout shown on the right inset).
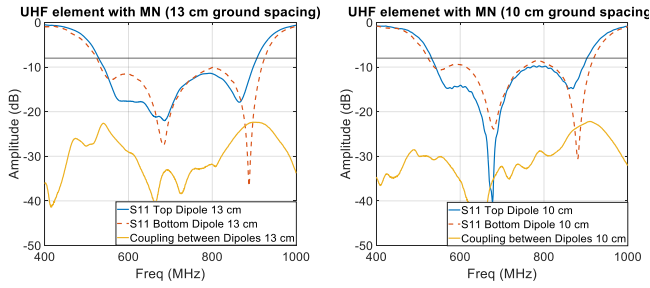
91

Fig. 8. Measured S-parameters of the UHF element inside its sled enclosure with matching networks attached.
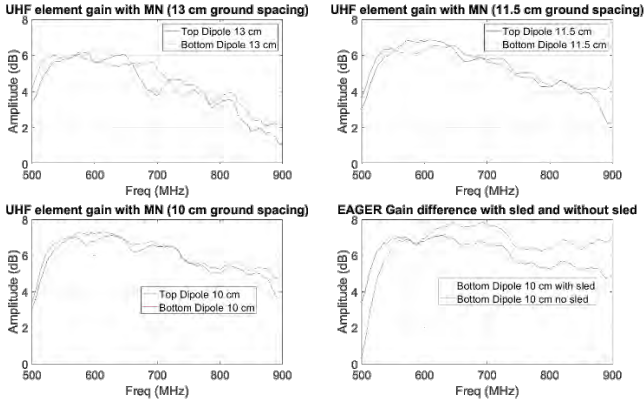

Fig. 9. Measured gain of the UHF element inside sled enclosure with matching networks attached.
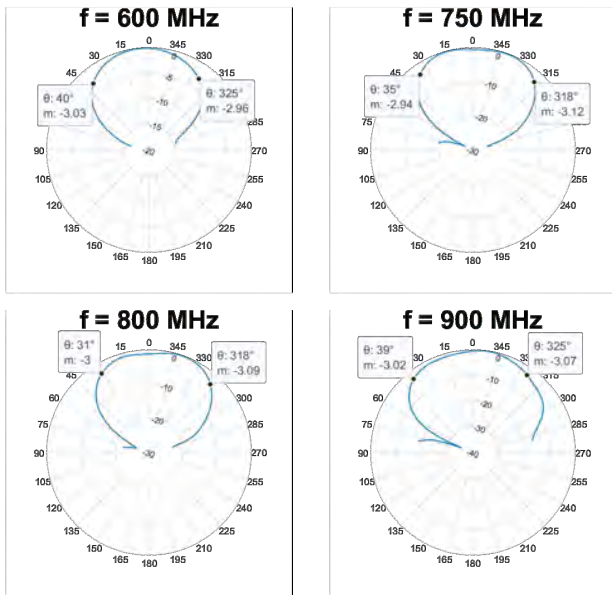

Fig. 10. Measured E-plane radiation patterns of the UHF antenna element within the sled.

Both UHF and VHF antenna systems are intended for installation inside rugged enclosures/sleds made of wood and plastic. These enclosures provide for environmental operation during field deployment. The sled containing the antennas will be towed by a vehicle (*e.g.,* snowmobile or tracked vehicle), which also carries the radar system. One such sled is designed to hold 16 UHF elements mounted on a plywood panel in the desired 4 x 4 configuration. The array is suspended 2.5 mm above the base of a plywood box sitting on top of a high-density polyethylene (HDPE) panel to ensure structural rigidity and ease of sliding when traveling through the rough snow terrain of Antarctica. The sled setup has an appreciable effect on performance, narrowing and shifting the 10-dB

return loss bandwidth to the left side of the frequency spectrum, as demonstrated in Fig. 6.

A third-order LC impedance matching network was designed using Keysight Genesys to feed each element and compensate for the adverse effect of the sled. Fig. 7 shows a photograph of the manufactured UHF antenna prototype with baluns and matching networks. The right inset shows the board layout of the matching network board. Fig. 8 and Fig. 9 demonstrate how the performance of the element changes with different ground plane height values. By reducing *H* to 10 cm (quarter wavelength at the center frequency) from the initial 13 cm, the return loss is slightly worse with two peaks slightly above -10 dB at 590 MHz and 784 MHz. However, this is still a considerable improvement over the losses in Fig. 6 for the unmatched case, since the 8-dB bandwidth with matching network now covers the entire required spectrum.

Keeping *H* = 10 cm is a reasonable tradeoff for the gain, given that on average the gains of top and bottom dipoles increased by about 2 dB and the drop across frequency is less severe (only a 1.9 dB variation across frequencies versus 3.5 dB). Overall, the UHF element with the new matching network and ground plane spacing has an actual bandwidth between 540 MHz and 900 MHz and a gain of roughly 6 dBi on average. This improvement in gain over that of a traditional dipole translates well into the radiation pattern in the E-plane (Fig. 10). The 3-dB beamwidth overall stays around 70 degrees across the bandwidth with no visible distortion. Compared to the beamwidth of a typical dipole (78 degrees), this reduction results in a more directed beam and hence the gain increase.

B. VHF Antenna Element

Tuning *L*, *L1*, *L2* and *L3* shows that the VHF antenna element performs best when the total length of the dipole is about 676 mm, or 80 % of the half wavelength at the center frequency (177.5 MHz). The S-parameters of the simulated model translate well into actual measurements with the use of the baluns and third-order matching networks. Both are designed using the same tools and methods presented in section III.A for the UHF element. The antenna element inside the sled structure is shown in Fig. 11.

The data in Fig. 12 demonstrate that this element resonates at two frequencies (143 MHz and 187 MHz, respectively), which combine to create a 10-dB bandwidth between 136.5 MHz to 203 MHz. Despite removing the notches along *L1*, the port-to-port isolation remains above 30 dB for the upper two-thirds of the bandwidth, while at worst reaching the same level as that of the original design [4].

Unlike the UHF matching networks, which only need to handle a maximum peak power of 400 W with up to 10 % duty cycle, the VHF elements must be able to withstand 1000 W peak with up to 12 % duty cycle. This makes the commercial-off-the-shelf (COTS) inductors *L1* and *L3* used in the initial prototype (rated for a maximum current of 1 A) particularly hot, reaching a temperature as high as 70 ºC at 800 W peak for the lowest frequency (140 MHz). This corresponds to a 47 ºC increase from room temperature at 80% load. To address this excessive temperature increase, we made custom wire wound inductors suitable for high power operation. We designed the high-power inductors using standard equations and manufactured them using 15 AWG gauge wire. We individually tuned each inductor against its COTS counterparts to achieve a nearly identical electrical response.
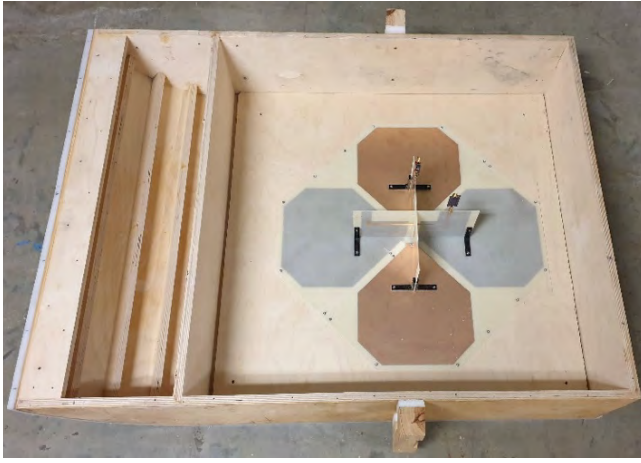
Fig. 11. Photograph of the final VHF prototype inside the sled with baluns and matching networks.
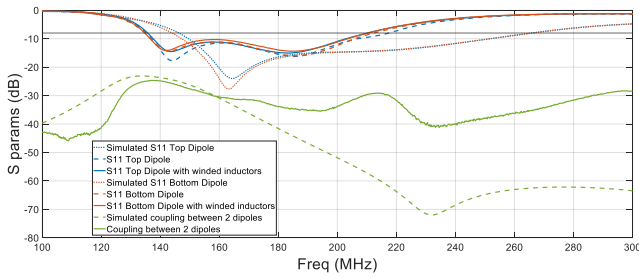

Fig. 12. Simulated and measured S-parameters of the VHF element inside sled enclosure with baluns and matching networks attached.
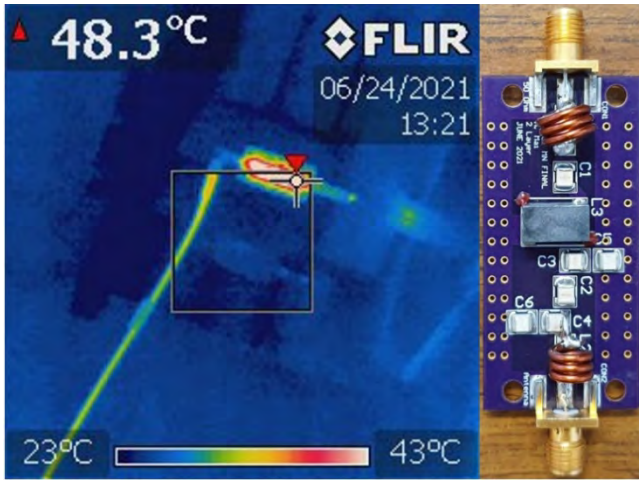

Fig. 13. Thermal image (left) of the VHF matching network with wire wound inductors (right) obtained inside an anechoic chamber under full RF load.
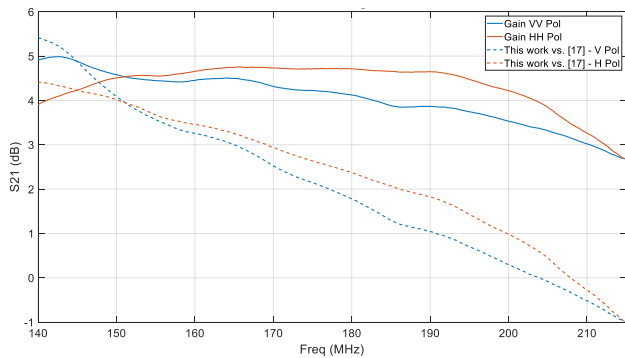

Fig. 14. Measured gain of the VHF element for both polarizations and comparison against an older single-polarization design.
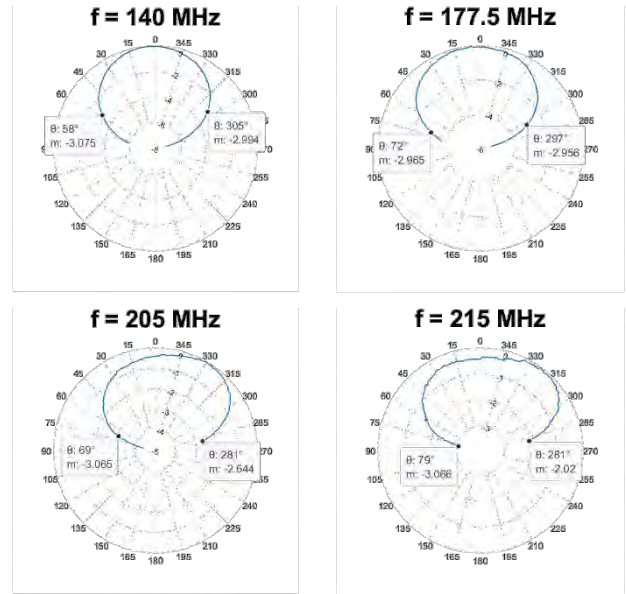

Fig. 15. Measured H-plane radiation patterns of the VHF antenna element within the sled.
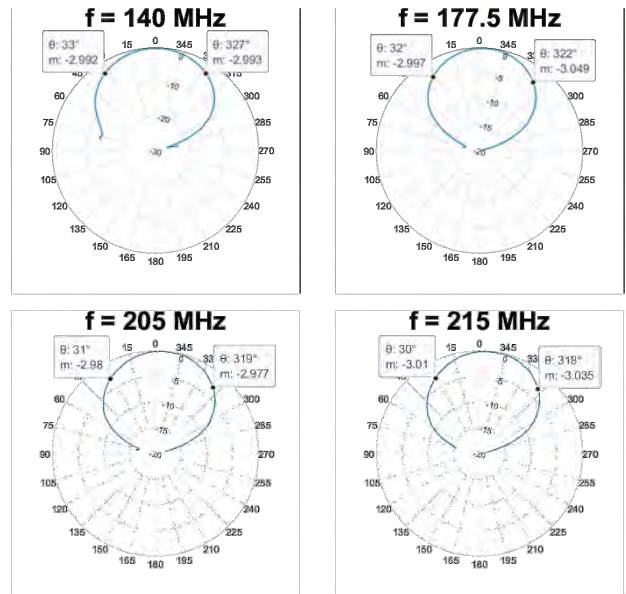

Fig. 16. Measured E-plane radiation patterns of the VHF antenna element within the sled.

This alteration not only maintained the level of electrical performance demonstrated in Fig. 12, but also brought down the inductor temperature to only 48 ºC under full 1000 W load applied to the antenna (Fig. 13). This corresponds to a modest 25 ºC change with respect to room temperature.

In its final configuration, the Band II element achieves an average gain of 4 and 4.35 dB for vertical (*V*) and horizontal (*H*) polarization, respectively. While the *V* polarization shows a constant decrease in gain over the frequency spectrum, the H polarization exhibits constant gain for up to two-thirds of the bandwidth before meeting the *V* polarization gain curve.

Next, we compared the measured gain values against the gain of an older single-polarization antenna design, which was used for an earlier sled-based experiment after adaptation from the polarization reconfigurable airborne configuration in [17]. Data from Fig. 14 illustrates that the VHF element's gain is up to ~ 5 dB higher (~2 dB on average) than that of

[17], which only outperforms our antenna very slightly (~1 dB) in the upper 10 MHz of the required band. It should also be noted that the gain variation across the entire bandwidth for the VHF element is only 2.3 dB, compared to 4.2 dB of the design in [17]. Moreover, this new design can support coincident dual-polarized measurements without reconfiguration.

Lastly, we will discuss the radiation patterns of the final VHF element. In the H-plane, the pattern is like a typical omnidirectional dipole antenna, in which the 3-dB beamwidth becomes wider as the frequency increases until it reaches 180º (Fig. 15). The difference lies in the E-plane pattern (Fig. 16), in which the 3-dB beamwidth starts at 66º and ends at 72º as the measurement frequency crosses the spectrum. This is considerably less than the 78º beamwidth of a typical half-wavelength dipole (hence the rise in gain) and is comparable to that of the original 1.7–2.7 GHz design in [4]. This behavior is expected, as the increase in E-plane beamwidth corresponds to a decrease in gain (less directive antenna) as the frequency augments.

IV. Conclusions and Future work

We designed, fabricated and tested a set of bi-polarimetric ultra-wideband antennas for ice mapping applications using VHF and UHF radar. The UHF element has a wide fractional bandwidth approaching 55 % with VSWR better than 2:1. We achieved good port-to-port isolation and acceptable gain and radiation patterns even on a sled platform for field measurements over snow/ice. The VHF element performed similarly with only a modest decrease in fractional bandwidth (43 %) with VSWR ≤ 2:1. The main trade-off we experienced was a decreased gain in favor of a better input match. Both antenna elements can withstand high peak power levels with duty cycles of up to 12 %. We provided a design methodology that can be adapted for other frequency bands by simply manipulating the parameters of each dipole and its associated balun and impedance matching network. Our newly developed antennas provide a cost-competitive solution for ultra-wideband radar ice sounding. Measured performance data demonstrates their suitability for the intended application. Future work includes the incorporation of multiple elements into an array, integration with the radar system, and field measurements in the Arctic and Antarctic in 2022.

References

[1] F. Rodriguez-Morales, D. Braaten, H. T. Mai, J. Paden, P. Gogineni, J-B Yan, A. Abe-Ouchi, S. Fujita, K. Kawamura, S. Tsutaki, B. Van Liefferinge, and K. Matsuoka, A Mobile, Multi-Channel, UWB Radar for Ice Core Drill Site Identification in East Antarctica: Development and First Results, *IEEE J. Sel. Top. App. Earth Obs. Remote Sens.*, vol. 13, 2020, pp. 4836-4847, 10.1109/JSTARS.2020.3016287.

[2] E. Arnold, C. Leuschen, F. Rodriguez-Morales, J. Li, J. Paden, R. Hale, and S. Keshmiri, CReSIS airborne radars and platforms for ice and snow sounding, *Ann. Glaciol.*, 2019, pp. 1–10. https://doi.org/10.1017/aog.2019.37.

[3] J. Paden, T. Akins, D. Dunson, C. Allen, and P. Gogineni, Ice-sheet bed 3-D tomography, *J. Glaciol.*, vol. 56, no. 195, 2010, pp. 3-11.

[4] Q.X. Chu, A Broadband +/- 45° Dual-Polarized Antenna With Y-Shaped Feeding Lines, *IEEE Trans. Ant. Prop.*, vol. 63, no. 2, Feb. 2015, pp 483-490.

[5] Y. Cui, R. Li and H. Fu, "A Broadband Dual-Polarized Planar Antenna for 2G/3G/LTE Base Stations," *IEEE Trans. Ant. Prop.*, vol. 62, no. 9, pp. 4836-4840, Sep. 2014, doi: 10.1109/TAP.2014.2330596.

[6] T. Feng, M. Su, Y. Liu and W. Wang, A Broadband Dual-Polarized Planar Antenna for LTE/5G Base Stations, *2019 IEEE 6th Int. Symp. Electromag. Comp.*, 2019, pp. 1-3, doi: 10.1109/ISEMC48616.2019.8986018.

[7] A. Tatomirescu and A. Badescu, Wideband Dual-Polarized VHF Antenna for Space Observation Applications, *Sensors*, 2020, 20, 4351.

[8] A. Fenn, P. Hurst, J. Sandora, J. Krieger, L. Parad, Low-Profile Dual-Polarized UHF Array Antenna, *2010 IEEE Int. Symp. Phased Arrays Syst. Tech.*, Oct. 2010.

[9] D. Inserra and G. Wen, Dual Orthogonal Port Stacked Patch Antenna With Vertical Pins for Simultaneous Transmit and Receive Applications, *IEEE Trans. Ant. Prop.*, 2021 (early access), 10.1109/TAP.2021.3090859.

[10] J. Huang, Z. Hussein, and A. Petros, A VHF Microstrip Antenna With Wide-Bandwidth and Dual-Polarization for Sea Ice Thickness Measurement, *IEEE Trans. Ant. Prop.*, vol. 55, no. 10, Oct. 2007, pp. 2718-2722.

[11] OPTION Wireless Technology. (2008, October). *OPTION Content Uploads.* Retrieved from OPTION Web Site: https://www.option.com/wp-content/uploads/2013/01/Option-White-Paper-Power-Considerations.pdf

[12] A. Haider and S.-H. Hwang. Maximum Transmit Power for UE in an LTE Small Cell Uplink, *Electronics,* 8 (2019): 796.

[13] Y. Huo, X. Dong and W. Xu, 5G Cellular User Equipment: From Theory to Practical Hardware Design, *IEEE Access*, vol. 5, pp. 13992-14010, 2017, doi: 10.1109/ACCESS.2017.272755

[14] R. Lee and M Zimmerman, Enhancement Of Array Gain With Stacked Parasitic Elements, *Proc. IEEE Ant. Prop. Soc. Int. Symp.*, 1994.

[15] K. Byers, A. Harish, S. Seguin, C. Leuschen, F. Rodriguez-Morales, H. Paden, E. Arnold, and R. Hale, A Modified Wideband Dipole Antenna for an Airborne VHF Ice-Penetrating Radar, *IEEE Trans. Instr. Meas.* vol. 61, no. 5, 2012, pp. 1435-1444.

[16] R. Bawer and J Wolfe, A Printed Circuit Balun for Use with Spiral Antennas, *IRE Trans. Microwave Theory Tech.* vol. 8, no. 3, 1960, pp. 319-325. Article.

[17] J.B. Yan, R. Hale, A. Mahmood, F. Rodriguez-Morales, C. Leuschen, S. Gogineni, A Polarization Reconfigurable Low-Profile Ultrawideband VHF/UHF Airborne Array for Fine-Resolution Sounding of Polar Ice Sheets, *IEEE Trans. Ant. Prop.,* vol. 63, no. 10, 2015, pp. 4334-4341.